Clocking convergence to a stable limit cycle of a periodically driven nonlinear pendulum

Mantas Landauskas[a] and Minvydas Ragulskis[b]
Research Group for Mathematical and Numerical Analysis of Dynamical Systems, Kaunas University of Technology, Studentu 50-222, Kaunas LT-51368, Lithuania

(Received 4 May 2012; accepted 14 August 2012; published online 30 August 2012)

Convergence to a stable limit cycle of a periodically driven nonlinear pendulum is analyzed in this paper. The concept of the H-rank of a scalar sequence is used for the assessment of transient processes of the system. The circle map is used to illustrate the complex structure of the manifold of non-asymptotic convergence to a fixed point. It is demonstrated that the manifold of non-asymptotic convergence to a stable limit cycle also exists in the stroboscopic representation of the transient data of the periodically driven nonlinear pendulum. A simple method based on a short external impulse is proposed for the control of transient processes when the transition time to stable limit cycles must be minimized. © *2012 American Institute of Physics*. [http://dx.doi.org/10.1063/1.4748856]

The Hankel rank (H-rank) of a scalar sequence reveals the complexity of the algebraic model describing the evolution of that sequence. The H-rank has been successfully used for the identification of manifolds of non-asymptotic convergence and for qualitative investigation of the onset of chaos for discrete nonlinear iterative maps. The pattern of H-ranks in the space of system's parameters and initial conditions is used for the demonstration that the manifold of non-asymptotic convergence exists in the stroboscopic representation of the transient data of the periodically driven nonlinear pendulum. This manifold is used for the construction of the control method of transient processes when the transition time to a stable limit cycle must be minimized.

I. INTRODUCTION

Clocking convergence is an important tool for investigating various aspects of nonlinear systems, especially chaotic maps. The rate of convergence to the critical attractor when a set of initial conditions is uniformly spread over the entire phase space may provide an insight of the fractal nature of the scale invariance of the dynamical attractor.[1,2] Numerical convergence of the discrete logistic map gauged with a finite computational accuracy is investigated in Ref. 3 where forward iterations are used to identify self-similar patterns in the region before the onset to chaos. A computational technique based on the concept of the H-rank is proposed in Ref. 4 for measuring the convergence of iterative chaotic maps. Computation and visualization of H-ranks in the space of system's parameters and initial conditions provides the insight into the embedded algebraic complexity of the nonlinear system and reveals three intertwined manifolds of discrete iterative maps: the stable manifold, the unstable manifold, and the manifold of the non-asymptotic convergence. It is shown in Ref. 4 that the computation of H-ranks can be effectively used for qualitative investigation of the onset of chaos for discrete nonlinear iterative maps.

There exist a whole range of analytical and numerical techniques for the analysis of the stability of limit cycles. The spectrum of Lyapunov exponents,[5,6] averaging methods,[7] and Floquet exponents[8–10] are successfully used for studying different properties of limit cycles. The main objective of this paper is to investigate the applicability of the concept of H-ranks for the assessment of the convergence processes to stable limit cycles.

This paper is organized as follows. The algorithm for the computation of the H-rank of a sequence and the concept of the manifold of non-asymptotic convergence are introduced in Sec. II. Computational identification of the manifold of non-asymptotic convergence is discussed in Sec. III; clocking convergence to a limit cycle is investigated in Sec. IV. A method for the control of transient processes is discussed in Sec. V; concluding remarks are given in the last section.

II. PRELIMINARIES

Let S is a sequence of real numbers

$$S := (x_0, x_1, x_2, \ldots). \tag{1}$$

The Hankel transform of S yields a sequence of determinants of Hankel catalectican matrices

$$d_n := \det(x_{i+j-2})_{1\le i,j\le n+1}, n = 0, 1, 2, \ldots \tag{2}$$

The H-rank of the sequence S is equal to m; $m \in N$ if

$$d_{m+k-1} = 0, \tag{3}$$

for all $k \in N$, but $d_{m-1} \neq 0$.[1] The existence of the H-rank is denoted by $HrS = m$.

Let us assume that $HrS = m$. Then S is a deterministic algebraic sequence and its elements are expressed in the following form:[11]

[a]Electronic mail: mantas.landauskas@ktu.lt.
[b]Electronic mail: minvydas.ragulskis@ktu.lt. URL: http://nonlinear.fmf.ktu.lt.

$$x_n = \sum_{k=1}^{r} \sum_{l=0}^{n_k-1} \mu_{kl} \binom{n}{l} \rho_k^{n-l}; n = 0, 1, 2, \ldots, \tag{4}$$

where the H-eigenvalues of the sequence $\rho_k \in C$, $k = 1, 2, \ldots, r$ can be determined from the Hankel characteristic equation

$$\begin{vmatrix} x_0 & x_1 & \cdots & x_m \\ x_1 & x_2 & \cdots & x_{m+1} \\ & & \cdots & \\ x_{m-1} & x_m & \cdots & x_{2m-1} \\ 1 & \rho & \cdots & \rho^m \end{vmatrix} = 0. \tag{5}$$

The recurrence indexes of these roots n_k $(n_k \in N)$ satisfy the equality $n_1 + n_2 + \cdots + n_r = m$. Coefficients $\mu_{kl} \in C$, $k = 1, 2, \ldots, r$, and $l = 0, 1, \ldots, n_k - 1$ can be determined from a system of linear algebraic equations which can be formed from equalities Eq. (4) (this system of linear equations has a unique solution).

Let us consider a discrete iterative system. The manifold of non-asymptotic convergence is defined as a set of initial conditions leading to a periodic regime in a finite number of forward iterations. Note that the whole set of initial conditions can be classified into the subset of initial conditions converging asymptotically to a stable periodic attractor (if only such an attractor exists) and the subset of initial conditions converging non-asymptotically to a periodic regime (stable or unstable).[1] The primary objective of this paper is to explore if the manifold of non-asymptotic convergence does exist in the stroboscopic representation of the model of a periodically driven pendulum.

III. THE MANIFOLD OF NON-ASYMPTOTIC CONVERGENCE AND THE *H*-RANK

As mentioned previously, the main objective of this paper is to show that the manifold of non-asymptotic convergence exists in the stroboscopic representation of the transient data of the periodically driven nonlinear pendulum. But before continuing with the model of the nonlinear pendulum we will demonstrate the functionality of the H-rank technique on the iterative circle map.

A periodically driven pendulum is one of the simplest physical systems whose dynamical description can be reduced to a circle map.[12–14] In its turn, the circle map is used in numerous models of nonlinear dynamical systems whenever the effects of quasiperiodicity are encountered.[15–18] The circle map is represented by the one-dimensional iterative map

$$\theta_{n+1} = f(\theta_n) = \theta_n + \Omega - \frac{K}{2\pi} \cdot \sin(2\pi\theta_n), \tag{6}$$

where θ is a polar angle (its value lies between 0 and 1), K is the coupling strength, Ω is the driving phase and $n = 0, 1, \ldots$. Initially we will investigate the circle map when Ω is set to 0.15 and K is varied in the interval $[0; \pi]$ (Figure 1(a)). We omit a considerable number of iterates ($k = 4000$) until initial transients terminates for every discrete value of K. The

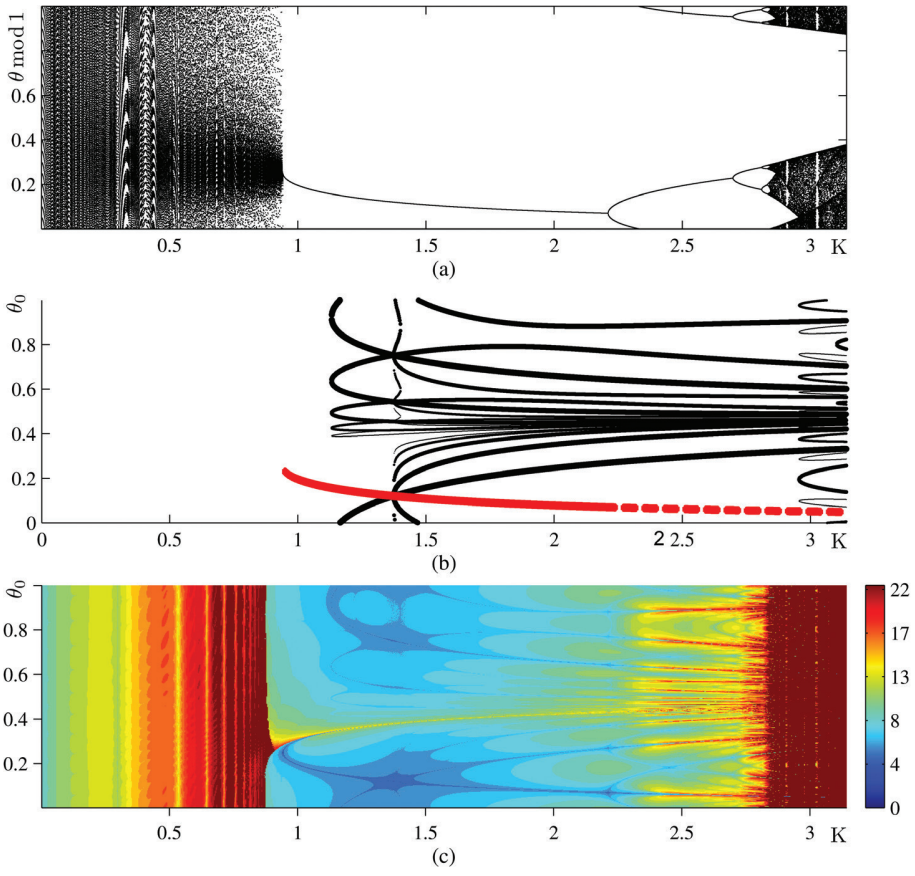

FIG. 1. The bifurcation diagram of the circle map is shown in part (a) at $\Omega = 0.15$. The manifold of non-asymptotic convergence to period-1 regime is illustrated in part (b). The thickness of black solid lines in (b) illustrates the number of forward iterations required to reach the period-1 regime; the red solid line stands for the stable period-1 regime; the red dashed line stands for the unstable period-1 regime which occurs after the first period-doubling bifurcation. The map of pseudoranks is shown in (c). All computations are performed at $\Omega = 0.15$.

rational number $\Omega = 0.15$ yields a periodic regime at $K = 0$. But the system experiences complex quasi-periodic transitions at increasing values of K until it falls into a stable period-1 mode (at K around 1). The further increase of K results into a cascade of period doubling bifurcations leading into the onset of chaos (Figure 1(a)).

Let us investigate the stable period-1 regime

$$\theta^\star = f(\theta^\star), \tag{7}$$

where $\theta^\star$ is the stable period-1 phase at $\Omega = 0.15$ and $K = 1$ (the stable period-1 regime exists then). The convergence to the stable period-1 regime can be asymptotic ($\lim_{n\to\infty} \theta_n = \theta^\star$) or non-asymptotic (when a finite number of forward iterations brings the system into the stable period-1 regime[4]). The non-asymptotic convergence to the stable period-1 regime can be explored by solving the inverse relationship

$$\theta_n = f^{-1}(\theta_{n+1}), \tag{8}$$

assuming that $\theta_{n+1} = \theta^\star$. Note that Eq. (8) can be iterated backwards for any number of steps. We exploit iterative nonlinear root finding algorithms (the bisection method and MATLAB software) for solving Eq. (8) since it is a transcendental equation. One backward step yields the value of θ_n bounded in the interval

$$\theta_n \in \left[\theta^\star - \Omega - \frac{K}{2\pi}, \theta^\star - \Omega + \frac{K}{2\pi}\right]. \tag{9}$$

If Eq. (8) has the only solution $\theta_n = \theta^\star$ then the manifold of the non-asymptotic convergence is an empty set. Such a situation is illustrated in Figure 2 where Figure 2(a) shows one backward iteration from $n = 0$ to $n = -1$. The root finding process of Eq. (8) is illustrated in Figure 2(b)—there do not exist other roots except $\theta^\star$ at $\Omega = 0.15$ and $K = 1$.

The situation becomes much more complex at $\Omega = 0.15$ and $K = 1.25$ (Figure 2(c)). It can be seen that Eq. (8) produces 3 roots; note that the root finding process is illustrated only for $n = -1$ in Figure 2(d). One root corresponds to the stable period-1 regime (the black line connecting the step number -1 with the step number 0 in Figure 2(c)). Another two roots represent such values of θ_{-1} which evolve into $\theta_0 = \theta^\star$ in one forward step (gray lines in Figure 2(c)). It is interesting to note that the continuation of backward iterations produces new roots grouped into two branches which tend to converge as the number of backward iterations increases. Thus, the manifold of non-asymptotic convergence is an infinite countable set of discreet initial conditions which lead to the stable period-1 regime in a finite number of forward iterations.

The root finding process becomes even more complex at $\Omega = 0.15$ and $K = 2.5$ (Figure 2(e)). Note that the middle root at $n = -1$ generates three roots at $n = -2$. Such a situation occurs only once; four different branches of backward roots tend to converge as backward iterations are continued. Finally, the situation becomes very complicated at $\Omega = 0.15$ and $K = 3$ (Figure 2(g)). Triples of backward roots are generated in an almost unpredictable manner as backward iterations are continued.

The manifold of the non-asymptotic convergence is visualized in Figure 1(b). The thick solid red line denotes the stable period-1 regime. The thick dashed red line represents the unstable period-1 regime which occurs after the first period-doubling bifurcation (Figure 1(a)). All black solid lines

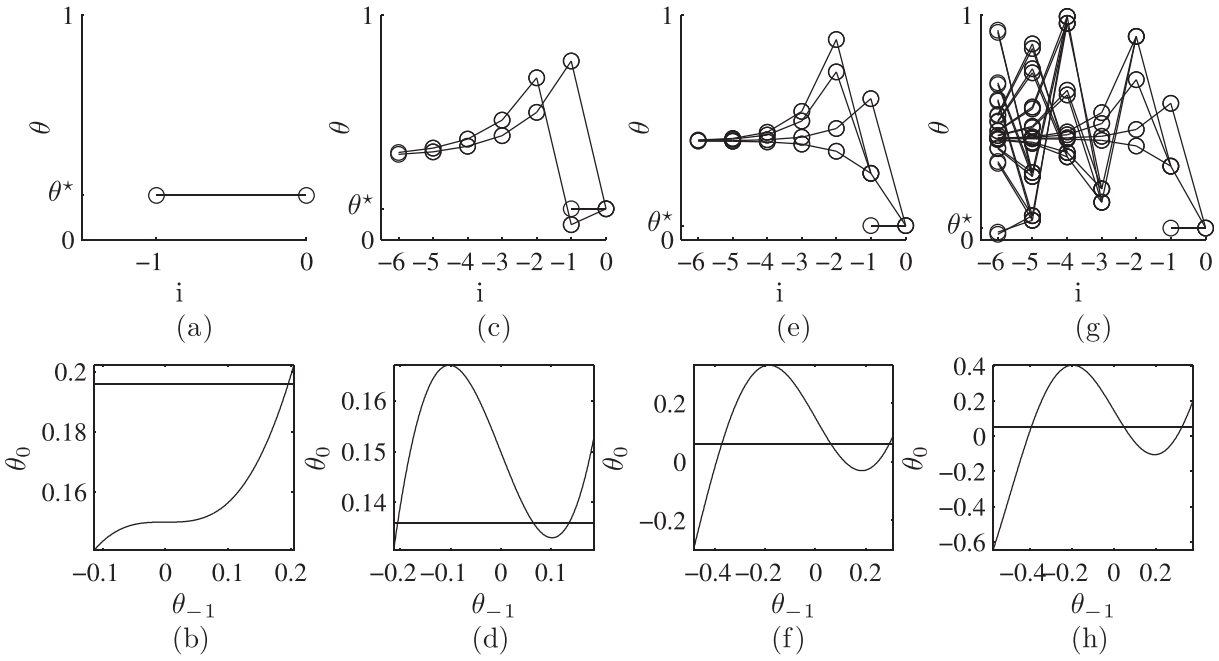

FIG. 2. The construction of the manifold of non-asymptotic convergence to the stable period-1 regime. There are no other initial conditions except the fixed point itself leading to the period-1 regime in a finite number of forward steps at $\Omega = 0.15$ and $K = 1$ (part (a)). Parts (c), (e), and (g) show the manifold at $\Omega = 0.15$, $K = 1.25$, $K = 2.5$, and $K = 3$ respectively. Parts (b), (d), (f), and (h) illustrate the root finding process: horizontal lines represent $\theta_0 = \theta^\star$; curved lines stand for $f(\theta_{-1})$.

represent the manifold of the non-asymptotic convergence to the period-1 regime (stable or unstable). The thickest black solid lines (the width is set to 6 pixels) illustrate initial conditions which result into the period-1 regime in one forward step. 5 pixels width black solid lines illustrate initial conditions which result into the period-1 regime in two forward steps; 4 pixels width lines—in three forward steps and so on. As mentioned previously, the interval of initial conditions $\theta_0 \in [0; 1]$ (at fixed Ω and K) can be classified into two sets: the infinite uncountable set of initial conditions converging asymptotically to $\theta^\star$ as n tends to infinity and the infinite countable set of initial conditions resulting into $\theta^\star$ in a finite number of forward steps (if only the stable period-1 regime exists). Figure 1(b) is a clear illustration of such a classification.

It has been shown in Ref. 4 that the H-rank can be used as an effective computational tool for the construction of the intertwined pattern of the stable, the unstable manifold and the manifold of the non-asymptotic convergence. We perform computational experiments for the circle map and compute H-ranks in the region $0 \le \theta_0 \le 1$ and $0 \le K \le \pi$ (at fixed $\Omega = 0.15$). For every pair of θ_0 and K we construct the sequence $(\theta_j; j = 0, 1, \ldots)$ and calculate the H-rank of that sequence. The results are shown in Figure 1(c). The manifold of the non-asymptotic convergence to the period-1 regime can be clearly seen in Figure 1(c) (the transient process is short due to the non-asymptotic convergence to the stable period-1 regime and thus the H-rank is low there).

The manifold of non-asymptotic convergence for the circle map (Figure 1(c)) is constructed using the computational technique based on H-ranks. One could raise a question if the manifold of non-asymptotic convergence could be constructed by performing a straightforward calculation of the number of steps of convergence to the stationary state instead.

In general, the applicability of the H-rank technique has a number of important advantages compared to the calculation of the number of steps. First of all, one does not have to consider the type of the stable attractor when applying the H-rank technique. Note that Figure 1(b) is constructed by counting backward steps from the period-1 regime (the construction of the manifold of non-asymptotic convergence to the period-2 stable regime would be much more complex). But the H-rank technique measures the complexity of transient processes; the manifold of non-asymptotic convergence is constructed simultaneously for all existing attractors.

Second, the H-rank technique automatically reveals the manifold of non-asymptotic convergence to unstable periodic regimes (if only they do exist). For example, a transient process can converge non-asymptotically to the unstable period-1 regime at $K = 2.5$ (Figure 1(c)). Backward iterations from the unstable period-1 regime allow the construction of the manifold of non-asymptotic convergence to the unstable fixed point (Figure 1(b)). But the identification of such non-asymptotic convergence would be complicated if the counting of forward steps would be used (simply because a stable period-2 regime and the unstable period-1 fixed point coexist at $K = 2.5$).

Finally, the H-rank technique allows identifying zones of regularity surrounded by complex chaotic processes in the parameter plane (at $K = 0.88$ and $K = 2.84$ in Figure 1(c)). Such identification would be nearly impossible using a straightforward calculation of the number of steps of convergence to a stationary state because the type of the attractor is not known at the beginning of the computational experiment.

IV. CLOCKING CONVERGENCE TO A LIMIT CYCLE

A periodically driven pendulum is a paradigmatic model in the study of oscillations and other phenomena in physics and nonlinear dynamics.[1] It has deserved much attention from many viewpoints including different model complexity, forcing, and damping aspects. We will use this model to explore the applicability of the H-rank for the investigation of the non-asymptotic convergence to the dynamical attractor. The model reads

$$\frac{d^2x}{dt^2} + b\frac{dx}{dt} + \sin x = f\cos(\omega t), \tag{10}$$

where t is time, x is the angular coordinate, b is the linear damping coefficient ($b > 0$), f and ω are the amplitude and the angular frequency of the harmonic forcing, respectively. Equation (10) exhibits rich chaotic behavior at $b = 1$. $f = 2.048$, and $\omega = \frac{2}{3}$ (Ref. 19): strobing at the drive frequency produces a cascade of period doubling bifurcations at $1 \le b \le 1.05$ (Figure 3). Values $f = 2.048$ and $\omega = \frac{2}{3}$ will be fixed in all further computations.

Note that the bifurcation diagram in Figure 3 is constructed from steady-state solutions (a considerable number of initial iterates are omitted in order to exclude the transient behavior of the system). On the opposite, the investigation of the convergence processes requires data on the transient behavior of the system. Therefore the computation of H-ranks for solutions of the periodically driven pendulum must be performed without omitting transient processes.

Let us consider a discrete partial solution computed using a constant-step time-forward marching integrator

$$x(t_0 + kh) = x_k, \quad \frac{dx}{dt}(t_0 + kh) = \dot{x}_k, \quad \frac{d^2x}{dt^2}(t_0 + kh) = \ddot{x}_k,$$

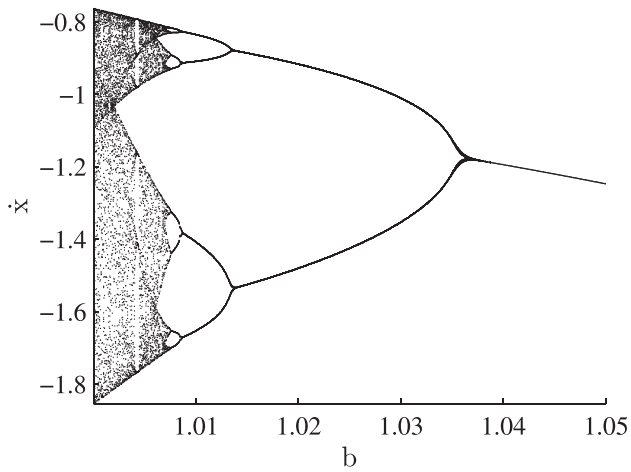

FIG. 3. The bifurcation diagram of the mathematical pendulum.

where $k = 0, 1, 2, \ldots$ and h is the integration step in time. A straightforward computation of the H-rank for the partial solution could be performed in several alternative ways: $Hr(x_0, x_1, x_2, \ldots)$, $Hr(\dot{x}_0, \dot{x}_1, \dot{x}_2, \ldots)$, $Hr(\ddot{x}_0, \ddot{x}_1, \ddot{x}_2, \ldots)$, or

$$Hr\left(\sqrt{x_0^2 + \dot{x}_0^2 + \ddot{x}_0^2}, \quad \sqrt{x_1^2 + \dot{x}_1^2 + \ddot{x}_1^2}, \quad \sqrt{x_2^2 + \dot{x}_2^2 + \ddot{x}_2^2}, \ldots\right). \tag{11}$$

Unfortunately, neither one of these strategies does yield interpretable results; the step of integration is too small to build a representative sequence from a short time series.

The alternative strategy for building a representative pattern of H-ranks could be based on Poincaré sections when the H-rank is computed from the sequence of consecutive coordinates of points in the section plane (Figure 4). Such computation of H-ranks for partial solutions reveals the intrinsic structure of intertwined manifolds, but the image is distorted due to inaccuracies in the determination of the point of intersection between the trajectory and the section plane (Figure 4).

Strobing at the drive frequency helps to overcome the up-mentioned drawbacks and the reproduced pattern of H-ranks reveals a clear structure of intertwined manifolds (Figure 5). It must be noted that a whole number of time steps must fit into the stroboscopic period; otherwise, the resulting pattern would be unclear due to the similar reasons as described above. Moreover, the numerical integrator must employ a constant-step time-forward marching technique; variable time step methods could not be used for the construction of patterns of H-ranks. We employ Newmark constant step constant average acceleration method;[20] the time step is set to $h = \frac{2\pi}{500\omega}$. Thus, every 500th step is used to construct the sequence and to calculate the H-rank as described by Eq. (11).

The fact that the rate of convergence to the limit cycle type attractor (at fixed parameters of the system) depends on initial conditions is not unexpected. The fact that the convergence to the stable limit cycle can be faster from a point located further away than from other point located nearer the limit cycle is also not astonishing. But the pattern of H-ranks reveals a clear structure of intertwined manifolds (compare Figure 5 to Figure 1(c) and to the pattern of H-ranks constructed for the logistic map in Ref. 1). The deepest trench (the lowest H-rank in Figure 5) corresponds to the initial condition near the trajectory of the limit cycle. But a number of "shadow" trenches are visible at other values of $\dot{x}_0$ in Figure 5. Note that the pattern of H-ranks is computed for the strobed data. Nevertheless, Figure 5 suggests that there exist a manifold of nonasymptotic convergence to the stable limit cycle in the stroboscopic representation of the transient data.

The interpretation of the pattern of H-ranks in Figures 5 and 6 can be illustrated by the following computational example. Let us consider the period-1 limit cycle at $b = 1.04$. Initial conditions $t_0 = 0$, $x_0 = \frac{371}{250}\pi \approx 4.660$, and $\dot{x}_0 = 0$ correspond to a point in the light blue region in the pattern of H-ranks in Figure 6. Transient processes are illustrated in Figure 7 (black dots denote strobing moments); (a) shows the evolution of process in the 3D coordinate system; (b) illustrates the projection of the transient process in the plane

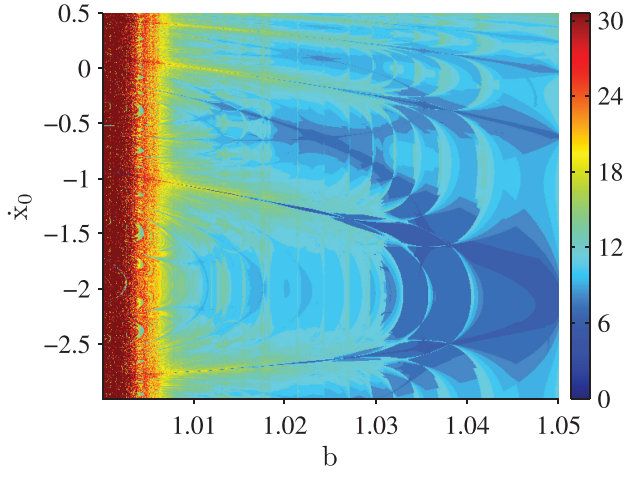

FIG. 4. The pattern of H-ranks for the system $\ddot{x} + b\dot{x} + \sin x = 2.048\cos\left(\frac{2}{3}t\right)$ ($x(0) = 0$ is fixed for all initial conditions). H-ranks are computed for sequences of Poincaré section points.

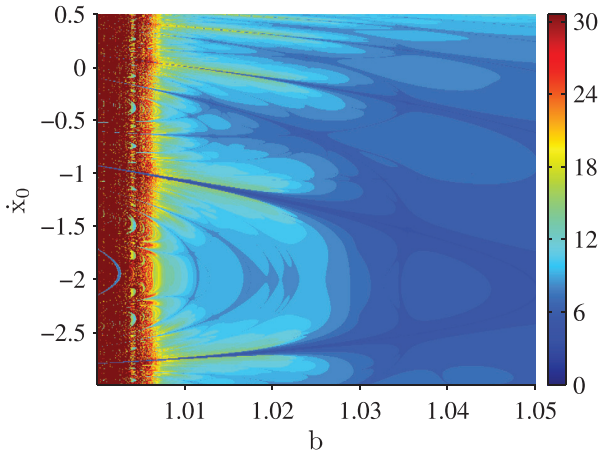

FIG. 5. The pattern of H-ranks for the system $\ddot{x} + b\dot{x} + \sin x = 2.048\cos\left(\frac{2}{3}t\right)$ ($x(0) = 0$ is fixed for all initial conditions). H-ranks are computed for sequences of the stroboscopic representation of the transient processes.

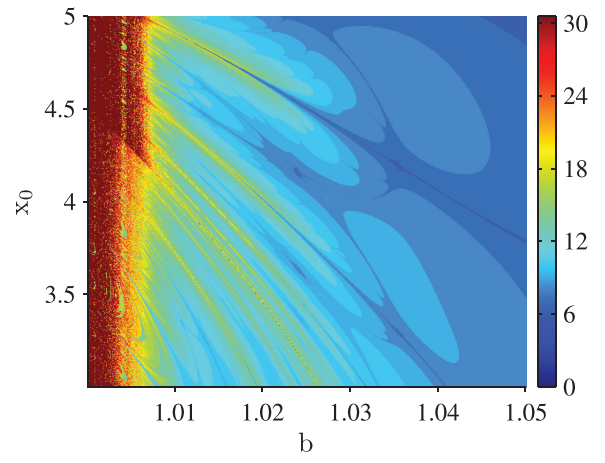

FIG. 6. The pattern of H-ranks for the system $\ddot{x} + b\dot{x} + \sin x = 2.048\cos\left(\frac{2}{3}t\right)$ ($\dot{x}(0) = 0$ is fixed for all initial conditions). H-ranks are computed for sequences of the stroboscopic representation of the transient processes.

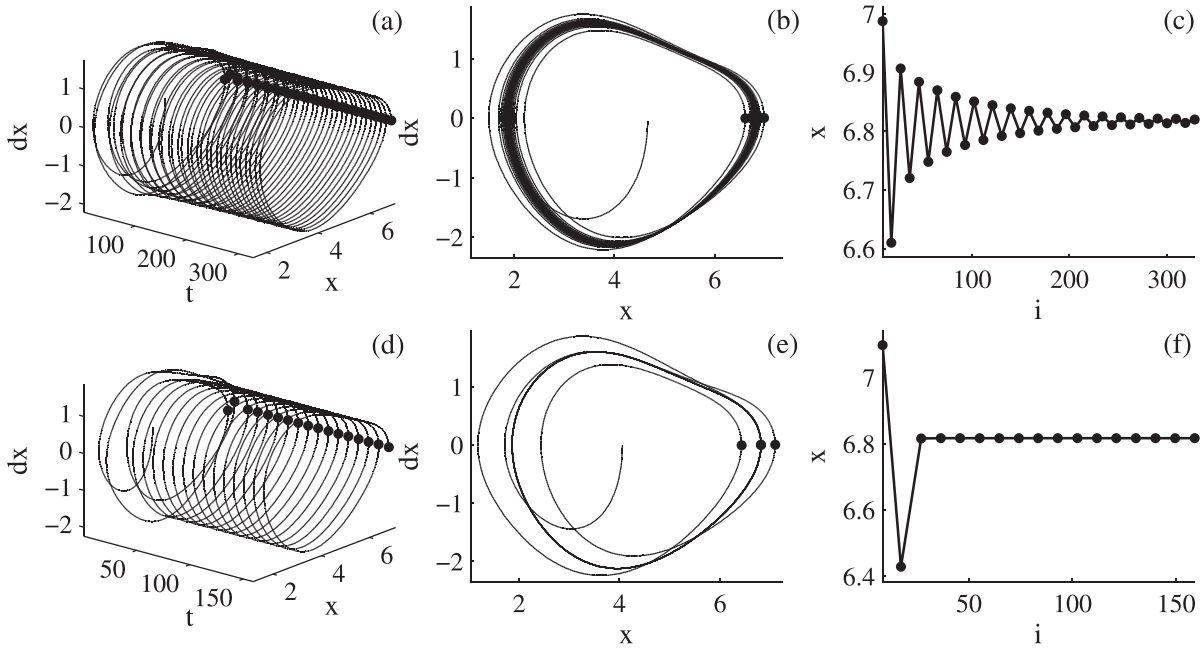

FIG. 7. Asymptotic versus non-asymptotic convergence to the stable limit cycle in the stroboscopic representation of the transient data of the system $\ddot{x} + b\dot{x} + \sin x = 2.048\cos\left(\frac{2}{3}t\right)$. Part (a) shows the evolution of the partial solution in 3D; (b) illustrates the projection of the transient process in the phase plane x–$\dot{x}$; (c) shows the consecutive sequence of strobing points starting from $t_0 = 0$; $x_0 = 4.66$, and $\dot{x}_0 = 0$. Parts (d), (e), and (f) illustrate the transient process starting from $t_0 = 0$, $x_0 = 4.059$, $\dot{x}_0 = 0$.

x–$\dot{x}$; (c) shows consecutive sequence of strobing points (adjacent strobing points are interconnected for the clarity only). It is clear that the transient trajectory converges asymptotically to the stable period-1 limit cycle.

The situation becomes different at $t_0 = 0$, $x_0 = \frac{323}{250}\pi \approx 4.059$, and $\dot{x}_0 = 0$ (Figure 7). These initial conditions correspond to the point in the deepest trench of the pattern of H-ranks in Figure 6. The transient process comprises three distinct loops; the system is locked into the period-1 attractor afterwards. Such transient dynamics can be explained by the nonasymptotic convergence to the period-1 limit cycle in the stroboscopic representation of the transient data.

V. CONTROL OF TRANSIENT PROCESSES

The existence of such special transient processes which yield fast nonasymptotic transitions to limit cycles enables the construction of effective control methods when the transition time must be minimized. It is shown in Ref. 1 that the whole set of initial conditions can be classified into the infinite uncountable set of initial conditions yielding asymptotic convergence to the stable fixed point and the infinite countable set of initial conditions yielding nonasymptotic convergence to the same fixed point. Thus a random selection of initial conditions most probably leads to the asymptotic convergence to the stable fixed point. Prior knowledge about the shape and the structure of the manifold of nonasymptotic convergence (as illustrated for the circle map for example) is required in order to select according initial conditions.

At this point it must be noted that the convergence to a stable limit cycle (in the strobed data) is considered now instead of the convergence to a fixed point. Let us consider the situation when the evolution of the system starts from initial conditions resulting into asymptotic convergence to a period-1 limit cycle ($b = 1.04$; all other parameters of the system are fixed throughout the computational experiment). Figures 5 and 6 represent patterns of H-ranks when one initial condition (x_0 or $\dot{x}_0$) is set to zero at $t_0 = 0$. These patterns would be different for other values of t_0, but they are exactly the same for $t_0 = \frac{2\pi}{\omega}k$, $k \in \mathbf{Z}$ due to the periodicity of the forcing term. Thus, patterns of H-ranks constructed for $t_0 = 0$ could be used for the control of transient processes at any time moment $t = \frac{2\pi}{\omega}k$, $k \in \mathbf{Z}$. Unfortunately, it is unrealistic to expect that one of the system variables ($x(t)$ or $\dot{x}(t)$) will become equal to zero at one of the strobing moments. A

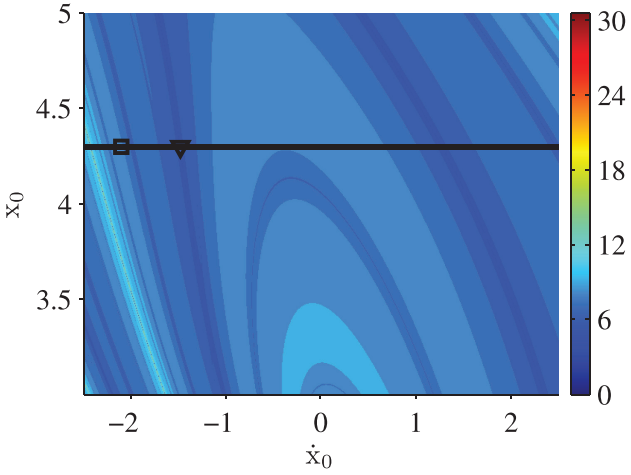

FIG. 8. The pattern of H-ranks for the system $\ddot{x} + b\dot{x} + \sin x = 2.048\cos\left(\frac{2}{3}t\right)$ in the phase plane $x_0 - \dot{x}_0$. The square marker denotes the position of the system before the impulse; the triangle marker—the position of the system after the impulse.

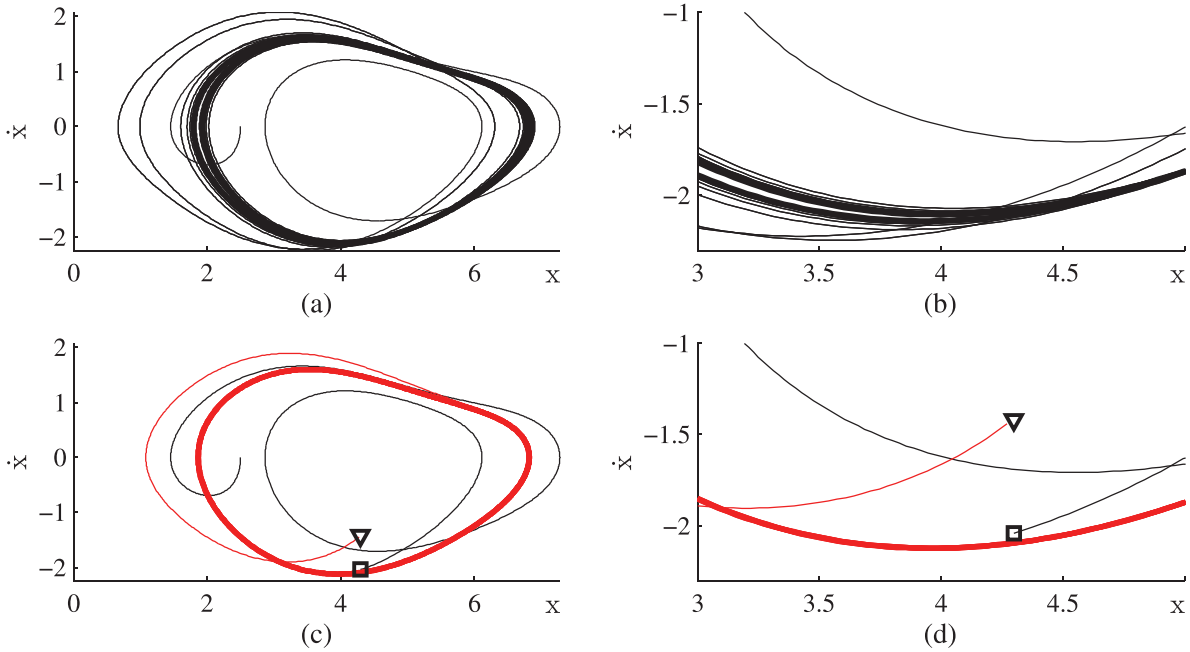

FIG. 9. The control of the transient process based on a single external impulse. The evolution of $\ddot{x} + b\dot{x} + \sin x = 2.048\cos\left(\frac{2}{3}t\right)$ starting from $x_0 = 2.5$ and $\dot{x}_0 = 0$ is shown in part (a). Part (b) shows the zoomed region of (a). The square marker denotes the position of the system before the impulse; the triangle marker—the position of the system after the impulse in part (c) (part (d) shows the zoomed region of (c)); the trajectory after the impulse is shown in red.

plot of H-ranks in respect of initial conditions x_0 or $\dot{x}_0$ (Figure 8) helps to resolve the above-mentioned limitation.

Let us assume that the transient process starts from initial conditions $x_0 = 2.5$; $\dot{x}_0 = 0$ (Figure 9(a)); the system converges asymptotically to the period-1 limit cycle; a zoomed region in Figure 9(b) illustrates the process of asymptotic convergence to the stable attractor. Figure 9(c) demonstrates the control technique based on a single control impulse (all system parameters including initial conditions are kept unchanged). The initial transient process (the black solid line in Figure 9(c)) is continued for two stroboscopic cycles. The system is then perturbed by an instantaneous impulse which changes the velocity (instantaneous the displacement remains unchanged). The position of the system before the impulse is denoted by a square and the position after the impulse—by a triangle in Figures 8 and 9(c). The magnitude of x before the impulse is marked by a thick black horizontal line in Figure 8; the triangle is placed in the nearest trench in the pattern of H-ranks in Figure 8.

VI. CONCLUDING REMARKS

It is demonstrated that the manifold of non-asymptotic convergence to a stable limit cycle exists in the stroboscopic representation of the transient data of the periodically driven nonlinear pendulum. Though the stable period-1 limit cycle was used for that purpose, similar phenomenon can be observed for stable limit cycles with higher periodicities.

The periodically driven nonlinear pendulum was used as a nonlinear model generating a stable periodic limit cycle. Similar effects could be observed in other nonlinear models of stable limit cycles, but a more detailed analysis of such systems remains a definite object of future research.

ACKNOWLEDGMENTS

Financial support from the Lithuanian Science Council under Project No. MIP-041/2011 is acknowledged.

[1]M. Ragulskis and Z. Navickas, Commun. Nonlinear Sci. Numer. Simul. **16**, 2894 (2011).
[2]F. A. B. F. de Moura, U. Tirnakli, and M. L. Lyra, Phys. Rev. E **62**, 6361 (2000).
[3]R. Tonelli and M. Coraddu, Eur. Phys. J. B **50**, 355 (2006).
[4]C. L. Bresten and J.-H. Jung, Commun. Nonlinear Sci. Numer. Simul. **14**, 3076 (2009).
[5]F. Christiansen and H. H. Rugh, Nonlinearity **10**, 1063 (1997).
[6]S. Habib and R. D. Ryne, Phys. Rev. Lett. **74**, 70 (1995).
[7]J. A. Sanders and F. Verhulst, *Averaging Methods in Nonlinear Dynamical Systems* (Springer, New York, 1985).
[8]C. Chicone, *Ordinary Differential Equations with Applications* (Springer, New York, 1999).
[9]P. Giesl, Nonlinear Anal. Theory, Methods Appl. **56**, 643 (2004).
[10]F. L. Traversa and F. Bonani, AEU Int. J. Electron. Commun. **66**, 357 (2012).
[11]Z. Navickas and L. Bikulciene, Math. Modell. Anal. **11**, 399 (2005).
[12]S. Ostlund, D. Randt, J. Sethna, and E. Siggia, Physica D **8**, 303 (1983).
[13]M. H. Jensen, P. Bak, and T. Bohr, Phys. Rev. Lett. **50**, 1637 (1983).
[14]M. H. Jensen, P. Bak, and T. Bohr, Phys. Rev. A **30**, 1960 (1984).
[15]M. McGuinness, Chaos **14**, 1 (2004).
[16]P. L. Boyland, Commun. Math. Phys. **106**, 353 (1986).
[17]F. Schilder and B. B. Peckham, J. Comput. Phys. **220**, 932 (2007).
[18]J. Escalona, J. V. José, and P. Tiesinga, Neurocomputing **44–46**, 91 (2002).
[19]R. C. Hilborn, *Chaos and Nonlinear Dynamics* (Oxford University Press, Oxford, 2000).
[20]N. M. Newmark, J. Eng. Mech. **85**, 67 (1959).